ESTEEM Academic Journal
Vol. 18, March 2022, 115-127

Boundary Extraction of Abnormality Region in Breast Mammography Image using Active Contours

Noor Ain Syazwani Mohd Ghani[1], Abdul Kadir Jumaat [2,*] and Rozi Mahmud[3]
[1,2]*Department of Mathematics, Faculty of Computer and Mathematical Sciences, Universiti Teknologi MARA, 40450, Shah Alam, Selangor, Malaysia*
[2] *Institute for Big Data Analytics and Artificial Intelligence (IBDAAI), Universiti Teknologi MARA, 40450, Shah Alam, Selangor, Malaysia*
[3]*Radiology Department, Faculty of Medicine and Health Sciences, Universiti Putra Malaysia, Serdang, Selangor, Malaysia*
**corresponding author: [2]abdulkadir@tmsk.uitm.edu.my*

ARTICLE HISTORY

Received
10 January 2022

Accepted
9 March 2022

Available online
31 March 2022

ABSTRACT

Mammography is a screening tool for breast cancer detection that produces grayscale images of the breast. The fundamental problem in mammography image analysis is to extract the boundary of breast abnormality from its healthy background tissues. The process is also known as the image segmentation. The procedure is necessary for further clinical diagnosis and monitoring in Computer Aided Detection (CAD) analysis systems. Active contour method has been proven to be effective to extract boundary of an image. The recent and effective selective type of active contour model, termed Primal Dual Selective Segmentation (PDSS) model, was proposed in 2019. However, the PDSS model having problem in segmenting images with low contrast. It is known that low contrast image is commonly encountered in mammography images that can result to poor boundary extraction. Thus, the aim of this study is to modify the PDSS model to extract the boundary of abnormality region in mammography images. The modification is made by considering three different image enhancement algorithms which are histogram equalization, histogram stretching and adaptive histogram equalization as the new fitting terms in the PDSS model and these results in three variants of modified PDSS models termed as PDSS1, PDSS2 and PDSS3 respectively. The efficiency of the proposed models was then assessed by recording the computation time while the accuracy of the extracted image boundary was evaluated using the Jaccard (JSC) and Dice Similarity Coefficients (DSC). Numerical experiments demonstrated that the proposed PDSS2 model based on histogram stretching achieved the highest segmentation accuracy with the fastest computational speed compared to other models. In future, the proposed model can be extended into the three-dimensional and colour formulations.

Keywords: *Active contour, boundary extraction, image enhancement, mammography images, selective segmentation.*

1. INTRODUCTIONS

Breast cancer has rapidly become the leading cause of mortality among women since 2018 which contributed to 15% from the total of 4.2 million female cancer deaths [1]. Currently, mammography is considered as a primary screening tool for breast cancer detection that produces a grayscale x-ray image of the breast. With the advance in computer technology, computer aided diagnosis (CAD) systems have been developed to assist or act as the second eye to radiologists, and the application of CAD has proven to improve the diagnostic accuracy of radiologists in cancer detection [2]. A CAD system can facilitate detection and

p-ISSN 1675-7939; e-ISSN 2289-4934

characterization of features such as shapes of breast lesions, microcalcifications and macrocalcifications which usually require the segmentation process.

Boundary extraction or also known as segmentation of mammography images in CAD system is a computational mathematical process used to precisely define the boundary of abnormality region before it can be classified as cancer or non-cancerous condition [3]. The segmentation approaches can be classified into level set and non-level set segmentation approaches. Level set approaches that are normally in variational framework use calculus of variations to minimize a cost energy functional where the basic idea is to define an objective function and apply optimization procedures to obtain optimality (minimum or maximum) while non-level set approaches that are normally derived in non-variational framework are formulated based on a heuristic approach [4].

Literature on the non-level set approach in extracting abnormality region mammography image is rich enough. For instance, [5] proposed a novel breast mass segmentation technique based on the combination of vector valued space and intensity variation analysis, while [6] introduced Fuzzy C-means algorithm to segment mammography images. More recently, deep learning-based technique [7] has also been applied to segment the breast region. The non-level set methods mentioned above are too dependent with number of data and type of data. For example, the deep learning-based techniques require various segmented training images which are not always available for mammograms [8].

The level set based segmentation approaches on the other hand are more structured approaches, can achieve high speed, accuracy, and stability in the performance [4, 9]. The level set based segmentation techniques can be classified into two main classes namely level set based global segmentation (global variational) and level set based selective segmentation (selective variational) approaches [10].

In the literature, the well- known active contour models are implemented by [11-12] on grayscale mammography images. The studies are for level set based global segmentation due to the fact that all features in an image are to be segmented. As such, this can result in a poor segmentation quality when the targeted abnormalities regions are too close or having almost similar intensities to healthy tissue boundaries, low contrast, fuzzy contour, and existence of noise. Level set based selective image segmentation which aims to extract one object of interest in an image based on some additional information of geometric constraints is more convenient to be used.

Selective segmentation is concerned with extracting or segmenting an object into a specific region with minimal user intervention [13]. In [14], a selective type active contour model namely Dual Level Set model was proposed. However, the model has a high computational complexity. Consequently, [15] improved the model and proposed one level set approach. The main issue with the model in [15] is sensitivity to initial solution due to non-convex formulation. As a result, [16] proposed Convex Distance Selective Segmentation (CDSS) model. This model performed better and more efficiently compared to the previous model as it is less sensitive to inputs from the user and has lower computational costs compared to [15].

Recently, Jumaat and Chen [10] proposed an effective selective type of active contour model, termed Primal Dual Selective Segmentation (PDSS) model. The model was found to be effective and efficient compared to the CDSS model [16]. However, the PDSS model is having

p-ISSN 1675-7939; e-ISSN 2289-4934

issues in segmenting images with low contrast. It is known that low contrast image is commonly encountered in mammography images that can result in a poor boundary extraction.

Different types of contrast enhancement techniques can produce different boundary extraction results, consequently affecting the segmentation accuracy. In MATLAB, three common enhancement techniques were included in the software namely histogram equalization, histogram stretching and adaptive histogram equalization.

Therefore, this study will propose selective type active contour models to effectively extract the boundary of breast abnormality in mammography images. This is done by reformulating the PDSS model where the fitting term in the respective model will be substituted with information from the image enhancement techniques namely histogram equalization, histogram stretching and adaptive histogram equalization algorithm. It is expected to improve in terms of image quality and segmentation accuracy by modifying the PDSS model.

The next part of this paper provides a brief review of the related models to this study, which is then followed by the formulations of the proposed models. The experimental results of existing and proposed models are then presented.

2. REVIEW ON THE PDSS MODEL

This Section 2 provides a brief review of the related models to this study.

2.1 Primal Dual Selective Segmentation (PDSS) Model

The selective segmentation model by Jumaat and Chen [10], namely the Primal Dual Selective Segmentation (PDSS), is an effective to implement compared to [15] and [16]. Let $z_0 = z_0(x,y)$ be an image in domain D. In the PDSS model, the marker set is introduced, and it is defined as $A = \{w_i = (x_i^*, y_i^*) \in D, 1 \le i \le n_1\}$ with $n_1(\ge 3)$ marker points that will be placed near the targeted object. The function $P_d(x,y)$ is the Euclidean distance of each point $(x,y) \in D$ from its nearest point in the polygon, P made up of $(x_p, y_p) \in P,$ constructed from the user input set, A. The function $P_d(x,y)$ is defined as the following Equation (1):

$$P_d(x,y) = \sqrt{(x - x_p)^2 + (y - y_p)^2}. \tag{1}$$

Then, the PDSS function is then defined as the following Equation 2:

$$\min_{u,w \in [0,1]} \left\{ PDSS(u,w) = \mu \int_D |\nabla u|_g \, dD + \int_D rw \, dD + \theta \int_D P_d w \, dD + \frac{1}{2\rho} \int_D (u - w)^2 \, dD \right\}. \tag{2}$$

Here, μ, θ and ρ are weightage parameters that control the total variation function $|\nabla u|_g$, distance function P_d and penalty term $(u-w)^2$ respectively. The function $g(x,y)$ is an edge detector function, the fitting term function r is given as $r = (b_1 - z_0)^2 - (b_2 - z_0)^2$ and w is a dual variable. The unknown constants b_1 and b_2 are the average intensity input image inside and outside of the contour u. The first term is the regularisation term to ensure the generated contour

p-ISSN 1675-7939; e-ISSN 2289-4934

or boundary of image, u smooth. The second term is the fitting terms to ensure the extracted boundary preserves the shape of the targeted abnormality region while the third term is the distance function to capture the targeted image boundary. The final term is the penalty term to ensure the solution u is close as possible to the dual variable w. The Equation (2) was solved using alternating minimization approach. While this method is effective for the selective segmentation model, it may give unsatisfactory results for an image with low contrast.

2.2 Histogram Equalization

The MATLAB software provide three image enhancement approaches namely histogram equalization, histogram stretching and adaptive histogram equalization algorithm. The function of histogram equalization is defined as the following Equation (3) in MATLAB:

$$z_{HE} = histeq(z_0). \tag{3}$$

Here, $z_0 = z_0(x, y)$ be an input image while z_{HE} is the output image using histogram equalization method. It enhances the contrast of images by transforming the values in an intensity image, z_0 so that the histogram of the output image approximately matches a specified histogram [17].

2.3 Histogram Stretching

In MATLAB, the function of histogram stretching is defined as the following Equation (4):

$$z_{HS} = imadjust(z_0). \tag{4}$$

Similarly, $z_0 = z_0(x, y)$ is an input image while z_{HS} is the output image using histogram stretching method. It increases the contrast of the input image, z_0 by mapping the values of the input intensity image to new values such that, 1% of the data is saturated at low and high intensities of the input data [18].

2.4 Adaptive Histogram Equalization

The method adaptive histogram equalization is defined as the following Equation (5):

$$z_{AHE} = adapthisteq(z_0). \tag{5}$$

Let $z_0 = z_0(x, y)$ is an input image while z_{AHE} is the output image using adaptive histogram equalization method. The method performs contrast-limited adaptive histogram equalization. Unlike histogram equalization method, adaptive histogram equalization operates on small data regions (tiles) rather than the entire image. Each tile's contrast is enhanced so that the histogram of each output region approximately matches the specified histogram [19].

p-ISSN 1675-7939; e-ISSN 2289-4934

3. THE PROPOSED MODELS

The PDSS model [10] may give unsatisfactory results for an image with low contrast. It will be modified by substituting the fitting term, z_0 in Equation (2) with the information from the image enhancement techniques i.e histogram equalization (z_{HE}), histogram stretching (z_{HS}) and adaptive histogram equalization (z_{AHE}) algorithm introduced in Equation (3), Equation (4) and Equation (5) respectively. Firstly, we introduce the modified PDSS model based on the histogram equalization (z_{HE}) of Equation (3), termed PDSS1. The modified model is defined as the following Equation (6): $\min_{u,w\in[0,1]} PDSS1(u,w)$,

$$PDSS1(u,w)=\mu\int_D\left(|\nabla u|_g+\left[(b_1-z_{HE})^2-(b_2-z_{HE})^2\right]w+\theta P_d w+\frac{1}{2\rho}(u-w)^2\right)dD. \quad (6)$$

Secondly, we define the modified PDSS model, termed PDSS2 that is formulated based on the histogram stretching (z_{HS}) of Equation (4). The second modified model is defined as the following Equation (7): $\min_{u,w\in[0,1]} PDSS2(u,w)$,

$$PDSS2(u,w)=\mu\int_D\left(|\nabla u|_g+\left[(b_1-z_{HS})^2-(b_2-z_{HS})^2\right]w+\theta P_d w+\frac{1}{2\rho}(u-w)^2\right)dD. \quad (7)$$

The third modified model termed PDSS3 demonstrates the substitution of the new fitting term generated from the adaptive histogram equalization method (z_{HS}) of Equation (5) into the PDSS model. The third modified model can be represented as the following Equation (8): $\min_{u,w\in[0,1]} PDSS3(u,w)$,

$$PDSS3(u,w)=\mu\int_D\left(|\nabla u|_g+\left[(b_1-z_{AHE})^2-(b_2-z_{AHE})^2\right]w+\theta P_d w+\frac{1}{2\rho}(u-w)^2\right)dD. \quad (8)$$

Similar in solving PDSS model, the alternating minimization method is applied to solve Equation (6), Equation (7) and Equation (8). The details of the scheme are well explained in [10, 13].

3.1 Steps of Algorithm for the Proposed Models

This algorithm shows the steps involved to implement the new proposed model, PDSS1 to compute the solution using MATLAB software.

1. Use command 'imread' in MATLAB to import mammography image.
2. Set the parameter values of μ, ρ, θ and define the marker set *A*.
3. Compute the solution of z_{HE} of Equation 3.
4. Initialize $n=0,$ thus $u^{(0)}, w^{(0)}$.
5. **For** $iter=1$ to maximum iterations, *maxit* or $\max\left(\frac{\|u^{n+1}-u^n\|}{\|u^n\|},\frac{\|w^{n+1}-w^n\|}{\|w^n\|}\right)\le tol$ **do**

p-ISSN 1675-7939; e-ISSN 2289-4934

Update $u^{(n)}, w^{(n)} \leftarrow \min_{u,w} PDSS1(u,w)$ of Equation 6 to $u^{(n+1)}$ and $w^{(n+1)}$ using alternating minimization method scheme [10,13].

end for

6. $u \leftarrow u^{(n)}, w \leftarrow w^{(n)}$. In practice, the output u will be defined as the final solution.

The stopping criteria used for this model is set as the value of tolerance, $tol = 1 \times 10^{-4}$. This process is repeated for the implementation of the other two modified models i.e.PDSS2 and PDSS3.

4. EXPERIMENTAL RESULTS

In this study, the value of $\mu = 1$, $\rho = 0.09$ are fixed for all problems. The value of θ varies between 300 to 4000 depending on the test images. Basically, the value of θ is large for object that is close to image noise or normal tissue, while a smaller value of θ is needed for the smooth object. The implementation was done using the MATLAB R2018 software. The CPU processor used was Intel(R) Celeron(R) CPU 3215U @ 1.70GHz with 4 GB installed memory (RAM).

There were 50 mammography images used in this experiment. Each of the images contain breast lesion. Figure 1 demonstrates the test images with markers in yellow to indicate the targeted object.

All the images in Figure 1 were obtained from INbreast database [20] which is publicly available dataset of breast cancer abnormalities. In addition, the images were cropped manually in MATLAB using *imcrop* tool at the region of interest (ROI) of size of 256 by 256 pixels to remove unnecessary information and to speed up the segmentation process.

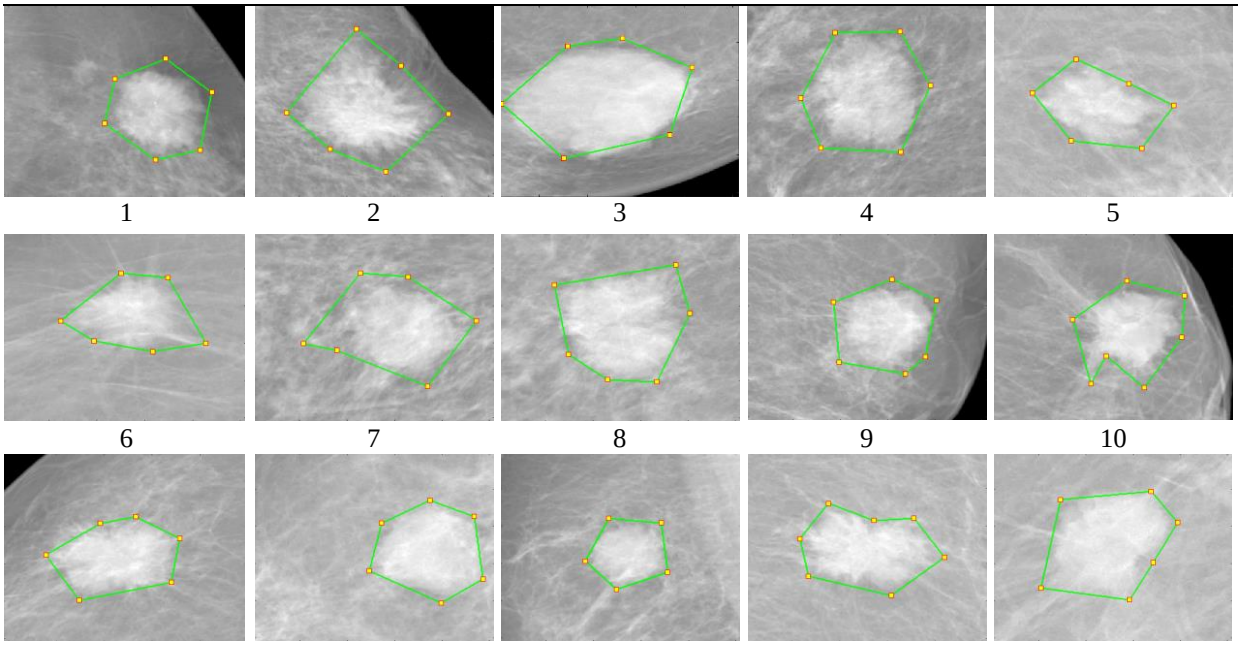

p-ISSN 1675-7939; e-ISSN 2289-4934

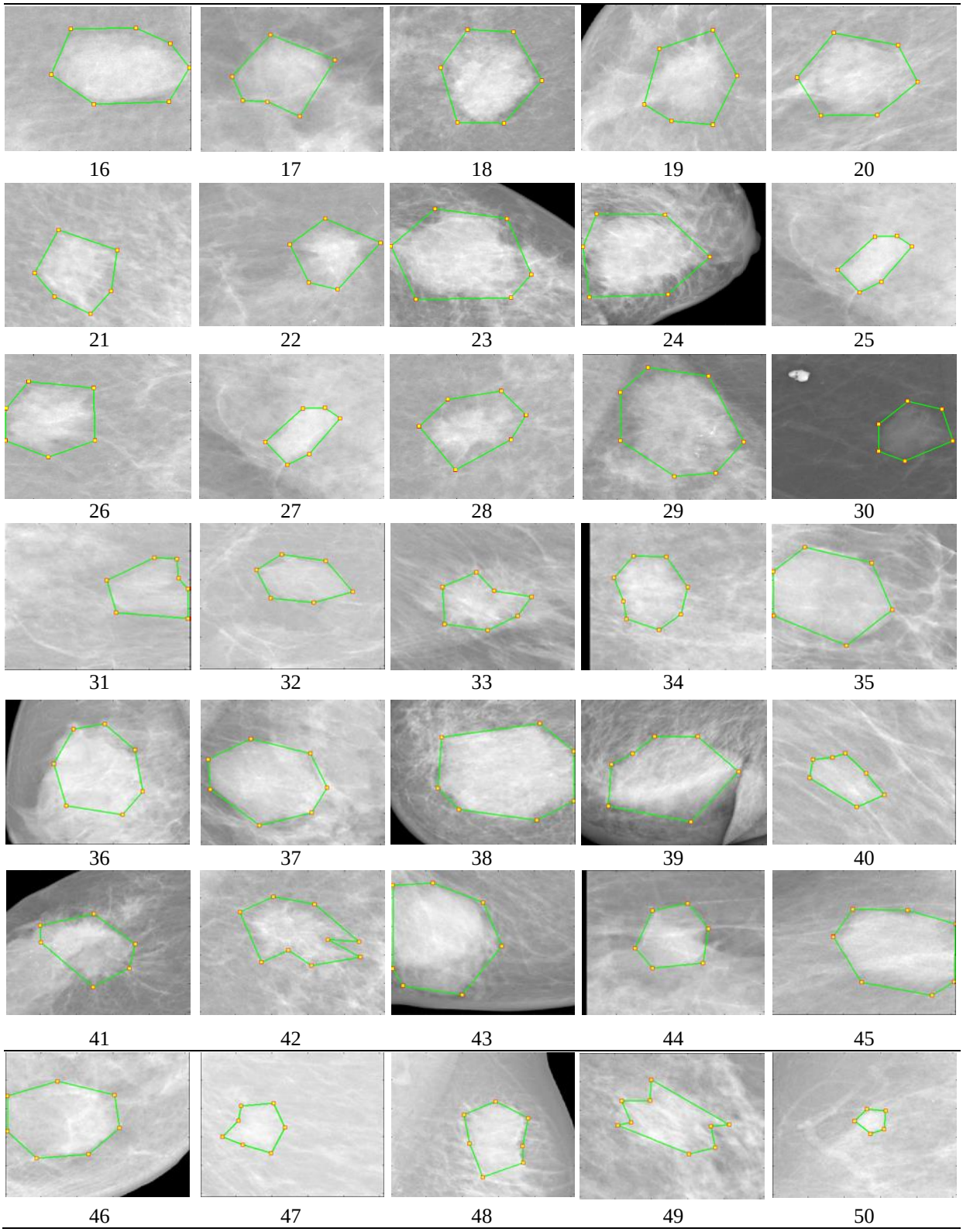

Figure 1: Test Images with Markers and Initial Contours

We remark that all these images were quite difficult to segment. This is due to the intensity inhomogeneity and irregularity boundaries in the images. This study compared the computational speed and accuracy of segmentation performance for PDSS model with the three

p-ISSN 1675-7939; e-ISSN 2289-4934

modified models that applied different enhancement technique known as PDSS1, PDSS2 and PDSS3.

Histogram equalization, histogram stretching, and adaptive histogram equalization algorithm are the three techniques of enhancement used in PDSS1, PDSS2 and PDSS3 respectively. Other than that, the segmentation performance for all models on 50 test images was compared by two approaches.

The first approach is known as qualitative approach where the segmentation performance of all models was assessed visually by eyeballing while the second approach is known as quantitative approach where two similarity coefficients namely Jaccard Similarity Coefficient (JSC) and Dice Similarity Coefficient (DSC) were computed in the models based on the following Equation (9):

$$\text{JSC} = \frac{|S_n \cap S_*|}{|S_n \cup S_*|}, \ \text{DSC} = \frac{|S_n \cap S_*|}{|S_n| + |S_*|} \tag{9}$$

where S_n is the set of extracted domains and S_* is the true set of extracted domains. The range of return value of the similarity function is in between 0 and 1. Figure 2 exhibits the segmentation results of each model for 6 out of 50 samples of chosen test images.

The results were in the form of curve representation (greyscale images with purple curve line). By visual observation from three modified models, PDSS2 model has a better segmentation result compared to PDSS1 and PDSS3 model. On the other hand, as we can see, the segmentation result of the existing PDSS model is nearly identical to the PDSS2 model.

However, PDSS2 model is capable of enhancing the contrast of the test images to expose detail information that is hidden in an image for better segmentation. In addition to qualitative analysis by visual observation, a quantitative analysis of the segmentation speed is also provided. Table 1 demonstrates the computation time (speed) of the segmentation results for each model.

Referring to Table 1, all 50 test images were compared for each model by recording the computation time. On average, PDSS2 model achieved the fastest computational speed in extracting the boundary of abnormality region compared to PDSS, PDSS1 and PDSS2 models.

In addition to computation speed, a quantitative analysis of the segmentation accuracy by evaluating the JSC and DSC values was also provided. Table 2 demonstrates the JSC and DSC values of segmentation results for each model.

Referring to Table 2, 50 test images were compared for each model to evaluate the JSC and DSC values. On average, PDSS2 model achieved the highest segmentation accuracy in segmenting the targeted objects compared to the other PDSS and PDSS1 models.

p-ISSN 1675-7939; e-ISSN 2289-4934

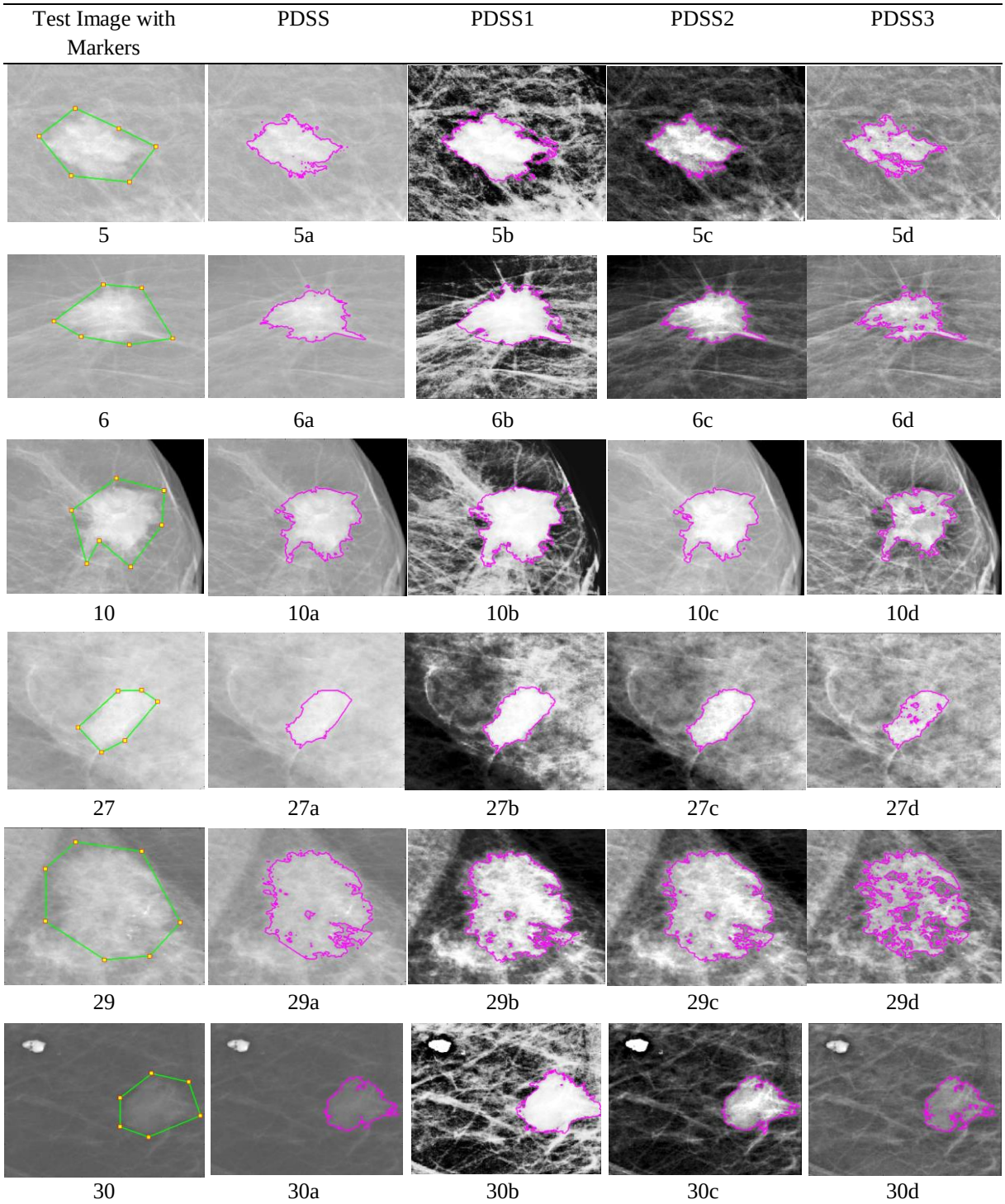

Figure 2: Boundary Extraction Results of 6 Samples of Test Images for PDSS with modified PDSS1, PDSS2 and PDSS3 models

p-ISSN 1675-7939; e-ISSN 2289-4934

Table 1: Computation Time for All Models

Test Images	Iteration				Time			
	PDSS	PDSS1	PDSS2	PDSS3	PDSS	PDSS1	PDSS2	PDSS3
1	9	10	7	8	107.95	149.08	89.65	114.27
2	9	7	7	7	107.69	102.74	94.24	91.71
3	10	9	7	7	119.88	140.94	97.16	91.67
4	9	6	7	7	108.12	87.61	99.89	91.11
5	9	7	7	7	107.80	121.98	99.59	84.86
6	9	7	8	8	108.13	91.33	97.32	102.87
7	14	7	8	9	166.00	86.19	109.51	116.50
8	8	7	8	8	97.36	96.80	106.97	95.65
9	12	7	7	7	144.31	96.72	96.26	91.54
10	9	9	7	52	108.83	120.11	94.73	633.27
11	7	6	7	9	84.84	73.53	84.90	109.96
12	7	6	7	7	84.83	82.46	73.63	90.85
13	7	6	7	6	85.31	77.54	86.03	80.79
14	9	9	9	7	108.39	117.26	109.53	92.50
15	8	6	7	7	97.29	79.17	92.43	92.05
16	8	9	7	7	97.24	114.53	84.52	92.16
17	9	6	7	13	102.34	120.32	228.55	98.97
18	10	9	8	8	123.29	108.35	104.79	97.01
19	9	24	8	12	142.52	293.95	106.99	146.13
20	13	10	9	8	156.19	121.19	115.16	110.10
21	9	6	7	8	109.30	91.74	86.45	103.59
22	9	8	8	9	111.70	97.29	107.84	119.29
23	15	7	6	7	180.06	84.90	73.22	97.78
24	6	7	6	7	73.13	94.41	81.84	88.87
25	8	8	7	8	183.94	120.72	86.05	103.98
26	12	7	8	8	196.49	92.36	103.97	105.84
27	7	7	7	7	86.02	86.81	91.48	85.37
28	9	7	9	8	119.70	90.97	108.93	113.80
29	9	8	7	8	160.81	157.56	116.8	142.7
30	10	7	8	8	148.44	93.71	107.5	115.22
31	13	8	8	8	148.90	93.06	92.57	93.88
32	9	7	8	7	103.92	82.56	95.54	82.78
33	8	6	6	7	92.77	72.66	70.19	82.53
34	7	7	7	7	81.91	81.73	81.50	84.14
35	7	7	7	8	81.27	81.81	81.34	95.58
36	6	6	6	6	67.49	66.35	63.38	67.92
37	8	7	7	8	87.75	77.50	77.02	87.35
38	6	7	6	8	68.63	78.35	67.26	89.01
39	7	6	6	42	77.01	67.62	67.36	6.09
40	7	6	7	8	78.08	67.50	77.84	88.95
41	7	7	8	8	77.83	78.19	89.16	89.62
42	11	7	8	8	121.30	78.80	89.26	89.31
43	8	7	8	7	88.51	78.42	89.05	79.27
44	8	8	9	8	89.34	89.24	99.85	103.17
45	7	6	6	8	110.23	133.22	103.77	164.61
46	7	8	7	8	135.45	131.08	116.43	112.53
47	14	7	7	8	169.81	85.60	85.45	96.15
48	6	7	6	6	73.44	85.68	73.68	73.71
49	7	7	6	8	85.34	85.51	73.75	97.91
50	11	7	7	7	133.08	85.64	87.48	85.56
Average	**8.9**	**7.5**	**7.2**	**9.3**	**111.98**	**98.82**	**91.74**	**108.64**

p-ISSN 1675-7939; e-ISSN 2289-4934

Table 2: JSC and DSC Values for All Models

Test Images	JSC PDSS	PDSS1	PDSS2	PDSS3	DSC PDSS	PDSS1	PDSS2	PDSS3
1	0.799	0.784	0.806	0.668	0.888	0.879	0.892	0.801
2	0.815	0.820	0.820	0.661	0.898	0.901	0.901	0.796
3	0.931	0.868	0.930	0.881	0.964	0.929	0.964	0.937
4	0.749	0.807	0.757	0.618	0.857	0.893	0.861	0.764
5	0.822	0.817	0.823	0.767	0.902	0.899	0.903	0.868
6	0.927	0.695	0.928	0.793	0.962	0.820	0.963	0.885
7	0.728	0.807	0.737	0.602	0.843	0.893	0.849	0.752
8	0.792	0.900	0.792	0.689	0.884	0.947	0.884	0.815
9	0.824	0.714	0.824	0.752	0.904	0.832	0.904	0.858
10	0.861	0.814	0.861	0.756	0.925	0.897	0.926	0.861
11	0.867	0.723	0.866	0.730	0.929	0.839	0.928	0.844
12	0.873	0.915	0.873	0.647	0.932	0.955	0.932	0.786
13	0.905	0.903	0.904	0.734	0.940	0.945	0.950	0.847
14	0.837	0.682	0.834	0.838	0.911	0.811	0.910	0.912
15	0.836	0.900	0.837	0.773	0.911	0.947	0.911	0.872
16	0.767	0.908	0.770	0.659	0.868	0.952	0.870	0.794
17	0.786	0.801	0.773	0.599	0.880	0.890	0.872	0.749
18	0.815	0.879	0.827	0.647	0.898	0.936	0.905	0.786
19	0.736	0.782	0.752	0.559	0.848	0.878	0.859	0.717
20	0.748	0.786	0.730	0.643	0.856	0.880	0.844	0.783
21	0.842	0.717	0.818	0.708	0.914	0.835	0.900	0.829
22	0.735	0.675	0.728	0.535	0.847	0.806	0.843	0.697
23	0.848	0.828	0.841	0.770	0.918	0.906	0.914	0.870
24	0.790	0.825	0.784	0.793	0.883	0.904	0.879	0.884
25	0.808	0.655	0.828	0.586	0.894	0.792	0.906	0.741
26	0.837	0.912	0.837	0.600	0.911	0.954	0.911	0.750
27	0.899	0.859	0.909	0.826	0.947	0.924	0.952	0.905
28	0.787	0.787	0.787	0.600	0.881	0.881	0.881	0.750
29	0.762	0.737	0.765	0.643	0.865	0.849	0.867	0.782
30	0.850	0.791	0.867	0.784	0.919	0.883	0.929	0.879
31	0.612	0.739	0.619	0.550	0.759	0.850	0.765	0.710
32	0.792	0.907	0.792	0.736	0.884	0.951	0.884	0.848
33	0.703	0.577	0.707	0.772	0.825	0.732	0.828	0.872
34	0.855	0.826	0.855	0.687	0.922	0.904	0.922	0.814
35	0.847	0.866	0.863	0.663	0.917	0.928	0.927	0.797
36	0.902	0.881	0.901	0.817	0.948	0.937	0.947	0.899
37	0.700	0.672	0.706	0.623	0.823	0.804	0.828	0.768
38	0.938	0.949	0.939	0.860	0.969	0.974	0.969	0.925
39	0.777	0.812	0.779	0.535	0.875	0.896	0.876	0.697
40	0.802	0.886	0.801	0.619	0.890	0.939	0.889	0.764
41	0.825	0.821	0.827	0.649	0.904	0.902	0.905	0.787
42	0.702	0.741	0.716	0.584	0.825	0.851	0.834	0.737
43	0.801	0.887	0.807	0.738	0.890	0.940	0.893	0.849
44	0.710	0.702	0.710	0.594	0.830	0.825	0.831	0.745
45	0.852	0.921	0.865	0.600	0.920	0.959	0.928	0.750
46	0.815	0.670	0.838	0.591	0.898	0.795	0.912	0.743
47	0.797	0.850	0.856	0.641	0.887	0.919	0.922	0.781
48	0.852	0.774	0.845	0.823	0.916	0.873	0.920	0.903
49	0.832	0.821	0.865	0.621	0.908	0.902	0.928	0.766
50	0.854	0.719	0.830	0.762	0.921	0.837	0.907	0.865
Average	**0.809**	**0.801**	**0.813**	**0.686**	**0.892**	**0.887**	**0.895**	**0.810**

p-ISSN 1675-7939; e-ISSN 2289-4934

5. CONCLUSION

In this research, we focused on selective type of active contour model to extract the boundary of abnormality region in grayscale mammography images. Three modified models were proposed in this research, i.e., PDSS1, PDSS2, PDSS3. To minimize the functional (what), the alternating minimization method [10,13] was implemented by developing the MATLAB coding. Then, the performance of each model was examined based on computational time and segmentation accuracy by evaluating JSC and DSC values for each image.

In the experiment, 50 images were presented to demonstrate the comparison of three modified models known as PDSS1, PDSS2, PDSS3 with the existing model of the PDSS. By visual observation, we found that PDSS2 model has a better segmentation result compared to PDSS1 and PDSS3 models. On the other hand, as we can see, the existing PDSS model's segmentation result is substantially identical to the PDSS2 model. However, PDSS2 model is capable of enhancing the contrast of the test images to reveal detailed information that is hidden in an image to get a better segmentation result. Besides, the computational time with JSC and DSC values were generated for all models to measure the segmentation performance. On average, PDSS2 model provides the highest segmentation result with fastest computational speed compared to PDSS, PDSS1 and PDSS3.

For further study, the recommended model i.e., the PDSS2 model can be extended into three-dimensional framework [21] and it can be extended in vector valued framework formulation for segmenting colour image. The reason is that vector valued (colour) and three-dimensional images consist of rich information and prominent intensity that can help in analysing medical or non-medical images. Since this research focuses on segmenting the breast lesions, it is worth exploring the performance comparison of the proposed model with [22-24] in segmenting the breast calcification. Moreover, it is recommended for future research to investigate the effects of changing different distance function such as [25] and the effects of changing different default values used in image enhancement algorithms towards the final segmentation output.

ACKNOWLEDGEMENT

This work was supported by the Ministry of Higher Education (MOHE) and Universiti Teknologi MARA, Shah Alam, grant number FRGS/1/2021/STG06/UITM/02/3.

REFERENCES

[1] F. Bray, J. Ferlay, I. Soerjomataram, R. L. Siegel, L. A. Torre, and A. Jemal, "Global cancer statistics 2018: GLOBOCAN estimates of incidence and mortality worldwide for 36 cancers in 185 countries" *CA. Cancer J. Clin.*, vol. 68, no. 6, pp. 394–424, 2018.

[2] R. Embong, M. H. Sanuddin, and M. S. Md Ali, "Staging of breast cancer based on the area of the primary tumour" *J. Phys. Conf. Ser.*, vol. 1366, no. 1, 2019.

[3] I. A. Ibachir, R. Es-salhi, I. Daoudi, S. Tallal, and H. Medromi, "A Survey on Segmentation Techniques of Mammogram Images" *Int. Symp. Ubiquitous Netw.*, vol. 1366, no. 1, 2016.

[4] A. B. Yearwood, "A Brief Survey on Variational Methods for Image Segmentation," pp. 1–7, 2010.

[5] B. Mughal, N. Muhammad, and M. Sharif, "Deviation analysis for texture segmentation of breast lesions in mammographic images" *Eur. Phys. J. Plus*, vol. 133, no. 11, 2018.

[6] R. Embong, N. M. N. Ab Aziz, A. H. Abd Karim, and M. R. Ibrahim, "Colour application on mammography image segmentation" *J. Phys. Conf. Ser.*, vol. 890, no. 1, 2017.

p-ISSN 1675-7939; e-ISSN 2289-4934

[7] K. J. Geras *et al.*, "High-Resolution Breast Cancer Screening with Multi-View Deep Convolutional Neural Networks" *arXiv Prepr. arXiv1703.07047.*, pp. 1–9, 2018.
[8] M. K. Sharma, M. Jas, V. Karale, A. Sadhu, and S. Mukhopadhyay, "Mammogram segmentation using multi-atlas deformable registration" *Comput. Biol. Med.*, vol. 110, pp. 244–253, 2019.
[9] T. Barbu, G. Marinoschi, C. Moroanu, and I. Munteanu, "Advances in Variational and Partial Differential Equation-Based Models for Image Processing and Computer Vision" *Math. Probl. Eng.*, vol. 2018, pp. 2–4, 2018.
[10] A. K. Jumaat and K. Chen, "A reformulated convex and selective variational image segmentation model and its fast multilevel algorithm" *Numer. Math.*, vol. 12, no. 2, pp. 403–437, 2019.
[11] N. S. Arikidis, V. Katerina, A. Kazantzi, S. G. Skiadopoulos, A. N. Karahaliou, and L. Castaridou, "A two-stage method for microcalcification cluster segmentation in mammography by deformable modelsNo Title" *Med. Phys.*, vol. 42, no. 10, pp. 5848–5861, 2015.
[12] Y. Guo *et al.*, "SCM-motivated enhanced CV model for mass segmentation from coarse-to-fine in digital mammography" *Multimed. Tools Appl.*, vol. 77, no. 18, pp. 24333–24352, 2018.
[13] A. K. Jumaat and K. Chen, "An Optimization Based Multilevel Algorithm for Variational Image Segmentation Models" *Electron. Trans. Numer. Anal.*, pp. 1–30, 2017.
[14] L. Rada and K. Chen, "A new variational model with dual level set functions for selective segmentation" *Commun. Comput. Phys.*, vol. 12, no. 1, pp. 261–283, 2012.
[15] L. Rada and K. Chen, "Improved selective segmentation model using one level-set" *J. Algorithms Comput. Technol.*, vol. 7, no. 4, pp. 509–540, 2013.
[16] J. Spencer and K. Chen, "A convex and selective variational model for image segmentation" *Commun. Math. Sci.*, vol. 13, no. 6, pp. 1453–1472, 2015.
[17] The MathWorks, Inc, *histeq*. Accessed on: Jan. 1, 2022. [Online]. Available: https://uk.mathworks.com/help/images/ref/histeq.html
[18] The MathWorks, Inc, *imadjust*. Accessed on: Jan. 1, 2022. [Online]. Available: https://uk.mathworks.com/help/images/ref/imadjust.html
[19] The MathWorks, Inc adapthisteq. Accessed on: Jan. 1, 2022. [Online]. Available: https://uk.mathworks.com/help/images/ref/adapthisteq.html
[20] I. C. Moreira, I. Amaral, I. Domingues, A. Cardoso, M. J. Cardoso, and J. S. Cardoso, "INbreast: Toward a Full-field Digital Mammographic Database" *Acad. Radiol.*, vol. 19, no. 2, pp. 236–248, 2012.
[21] A. K. Jumaat and K. Chen, "Three-dimensional convex and selective variational image segmentation model" *Malaysian Journal of Mathematical Sciences*., vol. 14, no 3, pp. 437–450, 2020.
[22] N. A. K. Zaman, W. E. Z. W. A. Rahman, A. K. Jumaat, and S. S. Yasiran, "Classification of breast abnormalities using artificial neural network" *In AIP Conference Proceedings*., pp. 1–7, 2015.
[23] S. S. Yasiran, A. K. Jumaat, M. Manaf, A. Ibrahim, W. E. Z. W.. A. Rahman, A. A. Malek, M. F. Laham, and R. Mahmud, "Comparison between gvf snake and ed snake in segmenting microcalcifications" *In IEEE Conference on Computer Applications and Industrial Electronics*., pp. 597–601, 2011.
[24] S. S. Yasiran, A. K. Jumaat, A. A. Malek, F. H. Hashim, N. D. Nasrir, S. N. A. S. Hassan, N. Ahmad, and R. Mahmud, "Microcalcifications segmentation using three edge detection techniques" *In International Conference on Electronic Devices, Systems, and Applications*., pp. 207–211, 2012.
[25] S. A. Abdullah and A. K. Jumaat, "Selective image segmentation models using three distance functions" *Journal of Information and Communication Technology*., vol. 21, no 1, pp. 95–116, 2022.

p-ISSN 1675-7939; e-ISSN 2289-4934